Novel bioresorbable tricalcium phosphate/polyhydroxyoctanoate (TCP/PHO) composites as scaffolds for bone tissue engineering applications

Ewelina Cichoń[a], Katarzyna Haraźna[b], Szymon Skibiński[a], Tomasz Witko[c], Aneta Zima[a], Anna Ślósarczyk[a], Małgorzata Zimowska[b], Małgorzata Witko[b], Bartosz Leszczyński[c], Andrzej Wróbel[c], Maciej Guzik[b,*]

[a] Faculty of Materials Science and Ceramics, AGH University of Science and Technology, Mickiewicza Av. 30, 30-059 Kraków, Poland
[b] Jerzy Haber Institute of Catalysis and Surface Chemistry Polish Academy of Sciences, Niezapominajek 8, 30-239 Kraków, Poland
[c] Faculty of Physics, Astronomy and Applied Computer Science, Jagiellonian University, Łojasiewicza 11, 30-348 Kraków, Poland

ABSTRACT

Development of new composite materials for bone tissue engineering is a constantly growing field of medicine. Therefore there is a continuous need in creating novel materials that can not only regenerate the defected tissue but also nourish it while the healing process progresses. Here we present a novel type of composite material that fulfils these requirements. The study describes creation of a composite with macroporous bioceramic core that is infiltrated with a thin biopolymer layer. The ceramic component, namely tricalcium phosphate (TCP), due to its mechanistic and bioactive properties may promote new bone creation as shown through the *in vitro* studies. To the best of our knowledge the coating layer was created for the first time from a representative of bacterially derived medium chain length polyhydroxyalkanoate polymers (mcl-PHA), namely polyhydroxyoctanoate (PHO). This polymer layer not only profoundly changed the stress-strain characteristics of the bioceramic foam but also released (*R*)-3-hydroxyacids and their dimers/trimers to the investigated environment. In the manuscript we have in depth characterised these materials employing a set of basic procedures, through 3D structure reconstruction and finishing with prolonged *in vitro* experiments.

1. Introduction

Tissue engineering is the field of regenerative medicine, which is developing constantly. One of its branches is bone tissue engineering (BTE), which encompasses among other fields the development of three-dimensional scaffolds used as supports in repair or regeneration of a damaged tissue. An ideal scaffold for BTE should be biocompatible, bioactive, osteoconductive or even osteoinductive in order to promote new tissue ingrowth. In addition, high interconnected porosity with the optimal pore size and their suitable architecture are required for optimal nutrient supply, cell attachment, migration and proliferation (Murphy et al., 2010; Sicchieri et al., 2012), maintaining appropriate mechanical properties at the same time. Another important feature of scaffolds for BTE is their optimal resorption, which fits the regeneration rate of the new-forming tissue (Hannink and Arts, 2011).

A wide range of biomaterials, including ceramics and polymers along with their manufacturing methods, have been proposed to meet the mentioned requirements (Winkler et al., 2018). Nowadays however, composite scaffolds, containing two or more different components, have been expected to provide enhanced functional and mechanical properties that the one-component implants were unable to meet. One of such approaches that drew scientists and clinicians attention is

fabrication and combination of bioglass or ceramic scaffold with biopolymer coating (Bretcanu et al., 2007; Fu et al., 2018).

Different types of calcium phosphate ceramics (CaPs), i.e. hydroxyapatite (HAp), α/β-tricalcium phosphate (α/β-TCP) or biphasic calcium phosphates [BCP (HAp/TCP)] are widely used in BTE due to their outstanding properties which promote bone tissue regeneration (Blokhuis et al., 2000). Properties of CaP ceramics depend mostly on the Ca/P ratio, crystallinity and phase composition. Coexistence of different phases gives possibilities to control resorption rate and biological response after implantation (Kamitakahara et al., 2008). CaPs such as α/β-tricalcium phosphate undergo a gradual degradation and resorption (as they are less stable than HAp) (Raynaud et al., 2002). In spite of these advantages, porous CaP ceramics exhibit poor mechanical properties (e.g. high brittleness and low compressive strength) limiting their range of applications. To counteract these drawbacks, coating the brittle scaffold with a thin layer of bioresorbable polymer gives the opportunity to toughen and even functionalise materials for BTE (Philippart et al., 2015).

A wide choice of synthetic (e.g. polycaprolactone (PCL), poly(lactic-co-glycolic acid) (PLGA), poly-DL-lactide (PDLLA) and natural (e.g. poly-3-hydroxybutyrate (PHB), alginate, silk and collagen) polymers have been proposed as coatings of ceramic scaffolds (Philippart et al.,

2015). Polyhydroxyalkanoates (PHAs) are natural polyesters produced by numerous microorganisms through bacterial fermentation of various carbon sources. Due to their excellent performance as biomaterials, they have attracted particular attention in the medical field (Gadgil et al., 2017). They not only can enhance structural properties of ceramics but also they nourish surrounding tissue through release of their degradation products – (R)-3-hydroxyacids – β oxidation intermediates (Goreva et al., 2012). What is more, a feature that differentiates PHAs from other biodegradable polymers such as PLA or PGA is degradation by the surface erosion, not by bulk hydrolysis (Gould et al., 1987) an important aspect if used as drug carriers, because of the wider control of drug release. PHO degradation is a very slow process, requiring several months of incubation. Its degradation rate can be increased dramatically by the introduction of polar carboxylic groups in the side chains, so it is quite tailorable (Renard et al., 2004). Polyhydroxyoctanoate (PHO) belongs to the medium chain length (mcl) PHAs polymer group. In contrast to brittle and stiff PHB – the most common type of PHAs, PHO is an elastomer with high extension to break (Poirier et al., 1995), which is important if considered for alteration of ceramics mechanical performance. PHO has only been studied as a material for soft tissue engineering, while the applications of PHO in BTE have not already been dealt with in depth (Ray et al., 2019). Application of this novel elastomeric polymer opens new routes for prolonged nourishing of the regenerating tissue. Moreover, further functionalisation with bioactive compounds for controlled drug release seems to be a promising application for PHO (Rossi et al., 2004).

In this study, we used PHO as a coating for CaPs ceramic scaffolds. Our main motivation was to employ this biodegradable and biocompatible elastomeric polymer in order to enhance mechanical and biological performance of the ceramic component, thus providing greatest implant integrity alongside nourishment of the developing tissue by a slow release of fatty acid degradation products. In this article we present simple manufacturing method of these composites with their physicochemical characterization (XRD, FTIR, porosity, surface and mechanical properties determination) and 3D scaffold reconstruction (micro CT). We performed *in vitro* studies in simulated body fluid (SBF) as well as prolonged hydrolytic degradation (SEM, PHO oligo/monomer release assayed *via* HPLC-MS).

2. Materials and methods

2.1. Powders preparation and characterization

β-TCP powder was synthesized by the wet chemical method described elsewhere (Ślósarczyk and Paszkiewicz, 2005). In brief $Ca(OH)_2$ (POCH, Poland) and H_3PO_4 (POCH, Poland) were used as starting materials. Analytically pure H_3PO_4 solution was dropped into Ca $(OH)_2$ suspension ($Ca/P = 1.5$) and the pH was kept near a value of 5-7. The precipitate was aged (24 h), centrifuged and dried. Obtained powder was ground in ball mill and sieved to grain size below 63 μm. We prepared two β-TCP powders: the first prepared as above and the second one additionally calcined at 900°C, ground in an attritor mill (4h), dried (90°C) and again sieved below 63 μm. Non-calcined and calcined powders were used for samples preparation. The specific surface area of the initial TCP powders was determined by Brunauer-–Emmett–Teller (BET) method using nitrogen (ASAP, 2000, Micrometric). Phase composition was characterized by X-ray diffractometry (XRD).

2.2. Microporous discs and macroporous foams preparation

Methods of preparing ceramic microporous discs (dTCP) and macroporous foams (fTCP) were optimized so that they would have a similar phase composition after sintering at 1200 °C. Firstly, for preliminary studies, non-calcined TCP powder (0.2 g for each specimen) was pressed under the pressure of 100 MPa into cylindrical microporous

samples (discs) (ø = 12 mm). Macroporous specimens (10 mm x 10 mm x 10 mm) were prepared by the polyurethane sponge replica method from slurries containing calcined β-TCP powder, with 0.37 g of liquid (distilled water with additives) for each gram of the powder (27% of liquid). In order to obtain smooth ceramic slurry and to increase its flow properties additives were included [0.14wt% methylcellulose; 4.1 wt% ammonium polyacrylate (Dispex A40)]. The slurry was then mixed thoroughly. Each sponge was immersed in ceramic slurry and squeezed to remove air. For each sponge, approximately 1.3 g of powder was used. The polyurethane sponges coated with the slurry were then dried at 60 °C for 2 h (note: obtaining relatively rigid foams was possible only with calcined powder). Next, all of the specimens were sintered in a conventional furnace for 3h at 1200 °C. Ceramic samples in the form of discs (dTCP) and foams (fTCP) were used as the reference material.

2.3. PHO synthesis and purification

Polyhydroxyoctanoate was obtained and purified as described previously (Sofińska et al., 2019). Briefly, *Pseudomonas putida* KT2440 was grown in a 5L fermentor on octanoic acid and minimal salt medium. Post fermentation biomass containing PHO polymer was dried and extracted with ethyl acetate. The polymer-ethyl acetate solution was purified over charcoal and filtered through 0.2 μm filter. PHO was precipitated in cold methanol and left to mature. For coating experiments, PHO was dissolved in ethyl acetate and three homogenous polymer solutions (2.5 wt% PHO; 5 wt% PHO; 10 wt% PHO) were prepared.

2.4. Composites preparation

Bioceramic discs were soaked in the polymer solutions (2.5; 5; or 10 wt% PHO) for 3 min, here referred to as dTCP/2.5PHO, dTCP/5PHO and dTCP/10PHO, respectively. Foams immersion was performed only in 5 wt% PHO solution (fTCP/PHO) as indicated by the preliminary studies with TCP discs. After evaporation of the solvent and drying at room temperature for 24 h, the composites were subjected to further studies.

2.5. Phase composition

The crystalline phases of sintered TCP powders as well as microporous discs and macroporous foams after sintering were analysed *via* powder X-ray diffraction (D2 Phaser diffractometer, Bruker). Also PHO and inorganic-organic disc were analysed after 2 weeks from preparation. The phase composition was determined using CuKα radiation (1.54 Å) with 30 kV and 10 mA. The intensity was recorded in 2θ range from 10° to 90° at 0.04° intervals with scanning speed of 2.5°min⁻¹. The crystalline phases were identified by comparing the experimental diffractograms to the Joint Committee on Powder Diffraction Standards: β-TCP (JCPDS 00-055-0898), α-TCP (JCPDS 00-009-0348). Quantitative phase composition analysis was performed using Profex (http://profex.doebelin.org) as a graphical user interface for the Rietveld refinement program BGMN (www.bgmn.de). (Doebelin and Kleeberg, 2015)

2.6. FTIR study

Fourier Transform Infrared (FTIR) spectra were recorded on a Tensor 27 Spectrophotometer, Bruker. The IR spectra were collected in the range of 4000-600 cm⁻¹ at a resolution of 4 cm⁻¹, 64 scans in ATR mode with diamond crystal.

2.7. Measurements of wetting angle

Wetting angle of obtained materials (dTCP, dTCP/PHO) was measured with Tensometer (Kruss DSA 100M) using water. Polymer

reference (PHO) was also included (glass coated with > 100 μm PHO layer). The test chamber temperature was controlled using a thermostatic water bath (22.0 ± 0.3 °C). For each material, more than 6 successive measurements were carried out.

2.8. Determination of surface free energy

The surface free energies were determined using an Owens Wendt (OW) method. The polar (γ_S^P) and dispersive (γ_S^D) components were calculated from the following equations:

$$\gamma_S = \gamma_S^D + \gamma_S^P$$

$$(\gamma_S^D)^{0.5} = \frac{\left[\gamma_d(\cos\Theta_d + 1) - \sqrt{\frac{\gamma_d^P}{\gamma_w^P}}\gamma_w(\cos\Theta_w + 1)\right]}{2\left[\sqrt{\gamma_d^D} - \sqrt{\gamma_d^P\frac{\gamma_w^D}{\gamma_w^P}}\right]}(\gamma_S^P)^{0.5}$$

$$= \frac{[\gamma_w(\cos\Theta_w + 1) - 2\sqrt{\gamma_S^D \cdot \gamma_w^D}]}{2\sqrt{\gamma_w^P}}$$

Where:

γ_S^D– the dispersive component of SFE of investigated sample,
γ_S^P– the polar component of SFE of investigated sample,
γ_d– the SFE of diiodomethane (50.8 mN m-1),
γ_d^D– the dispersive component of diiodomethane surface energy (48.5 mN m^{-1}),
γ_d^P– the polar component of diiodomethane SFE (2.3 mN m^{-1}),
γ_w– the SFE of water (72.8 mN m^{-1}),
γ_w^d– the dispersive component of water SFE (21.8 mN m^{-1}),
γ_w^P– the polar component of water SFE (51.0 mN m^{-1}),
θ_d– the contact angle of diiodomethane,
θ_w– the contact angle of water.

2.9. Surface morphology and pore architecture observations

The surface of prepared discs as well as foams pore architecture were observed under the optical microscope (Leica DM2500M). Pore architecture and infiltration efficiency were analysed using μCT (Bruker SkyScan 1172 micro-CT scanner). Scanning parameters were set to optimize the signal to noise ratio where the X-ray energy was set to 80 keV and 0.5 mm Al filter was applied. Images were scanned at a pixel size of 5 μm. Image reconstruction procedure was applied using a modified Feldkamp algorithm build in Nrecon software (Bruker Micro-CT). All samples were visualized with 3D volume rendering method using CTVox package (Bruker Micro-CT) with an optimized transfer function. In order to accurately depict the efficiency of infiltration, 1 wt % of X-ray contrasting component – iodobenzene (IB) was added to the polymer solution. In that way, PHO with IB addition was more visible on scans (blue colour) as iodine is a heavy element and iodine-based contrasts are commonly used in μCT studies (Garcea et al., 2018). In order to ensure that the ceramics do not absorb iodine from iodobenzene, μCT scans of fTCP (immersed in ethyl acetate solution with IB addition) have also been made. As the references, fTCP and fTCP/PHO samples without iodine were scanned.

2.10. Microstructure and chemical analysis in microareas

Microstructure and chemical analysis of obtained materials before and after degradation studies was investigated using a scanning electron microscope (Nova 200 NanoSEM) equipped with FEI Co. EDS system. Observation of microstructure and chemical composition analysis of samples after incubation in SBF were carried out by means of JEOL JSM – 7500F Field Emission Scanning Electron Microscope equipped with Retractable Backscattered-Electron detector (RBEI) and EDS (energy dispersive spectra) detection system of characteristic X-ray radiation INCA PentaFetx3 EDS system.

2.11. Porosity studies

Ceramic and composite foams were subjected to porosity measurements. Apparent density, open and total porosity were measured by hydrostatic weighing (Archimedes' method – AM). Moreover, porosity was also calculated from μCT scans.

2.12. Compressive strength measurements

The compressive strength of composites was measured using Instron testing machine (Model: 3345) and was determined in uniaxial compression tests, using 1.0 mm min^{-1} crosshead speed. The foam samples in the cubic form with dimensions of 9-10 mm x 9-10 mm were used. In all mechanical determinations, results were based on an average of 10 samples.

2.13. Degradation studies

For degradation studies, specimens in the form of discs were used. Investigated materials were stored in the environment of distilled water at 37 °C in polypropylene (PP) containers. During the experiment pH and conductivity of water were measured to determine chemical stability of the materials. After 3-month incubation discs were dried and subjected to microstructure analysis. Residual water from each of the container was subjected to HPLC-MS analysis to qualitatively determine the products of degradation.

2.14. Chemical stability and in vitro bioactivity studies

Ceramic and composite discs were placed into the PP container with 40 mL of SBF prepared according to Kokubo method (Kokubo, 2008) and stored at 37 °C till 21 days. During the experiment, pH of SBF were measured to determine chemical stability of the materials. After the pre-selected soaking time in SBF the samples were gently rinsed with distilled water to remove residual SBF solution followed by drying at 40 °C. Sample surfaces after 21-day incubation were characterized by SEM and EDS for evaluation of *in vitro* bioactivity.

2.15. HPLC-MS measurements

Liquid samples (10 ml) were lyophilized and extracts suspended in 1 ml methanol, filtered and analyzed on Agilent 1290 Infinity System with automatic autosampler and MS Agilent 6460 Triple Quad Detector equipped with Agilent Zorbax Eclipse Plus C18 column (2.1 x 50 mm, 1.8 μm). Samples were developed on the column at 30°C at a flow rate of 0.4 ml min^{-1} and with gradient elution of solvent A (0.1% v/v formic acid in water) and solvent B (0.1% v/v formic acid in acetonitrile) as follows: 0.00 min (50% A/50% B) to 1.90 min (10% A/90% B) to 1.91 min (50% A/50% B) to 2.60 min (50% A/50% B). The injection interval was 2.6 min. MS Agilent 6460 Triple Quad tandem mass spectrometer with Agilent Jet Stream ESI interface was used in negative ion mode. Nitrogen at a flow rate of 10 l min^{-1} was used as the drying gas and for collision-activated dissociation. Drying gas and sheath gas temperatures were set to 350°C. Capillary voltage was set to 3500 V, whereas the nozzle voltage was set to 500 V. Elution profiles were monitored in a scan range of 50-1000 m/z first in order to determine main peaks. Next, main degradation compounds were monitored in multiple reaction monitoring mode (MRM) with the following transitions, polarity, fragmentor (F) and collision energies (CE): ESI-: (R)-3-hydrohexanoic acid 131.1→59.1m/z, F = 83V, CE = 6V; (R)-3-hydroxyoctanoic acid 159.1→59.1 m/z, F = 63V, CE = 10V; dimer (R)-3-hydroxyoctanoic-(R)-3-hydrohexanoic acid 273.1→131.1 m/z, F = 68V, CE = 6V; dimer (R)-3-hydroxyoctanoic-(R)-3-
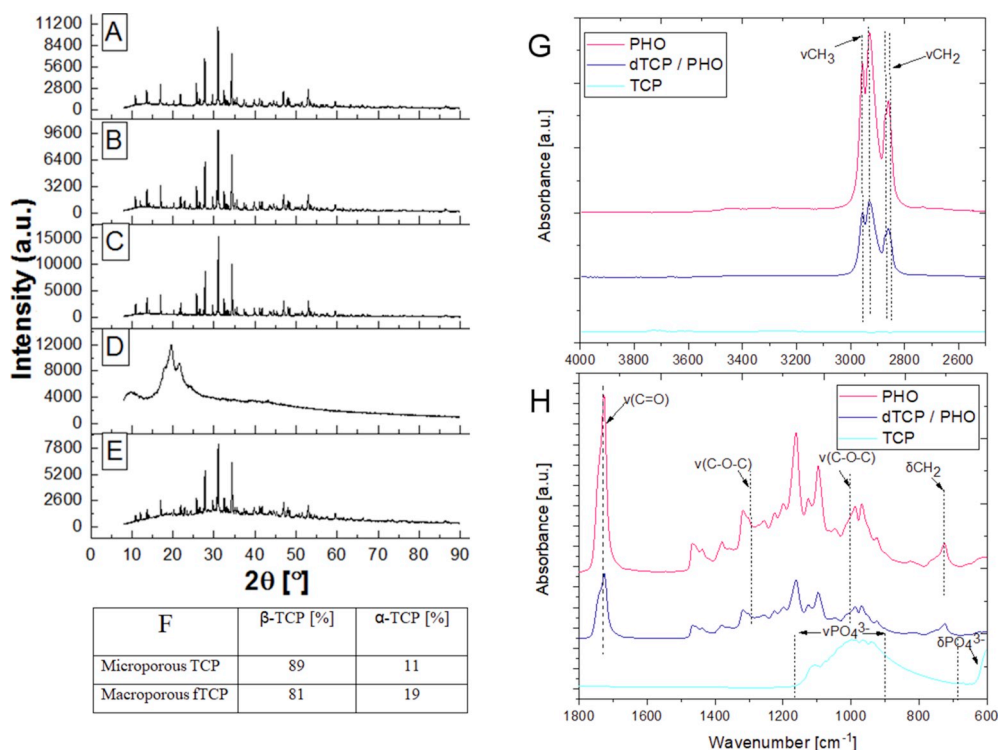
Fig. 1. Diffractograms of: A) initial powder calcined at 900 °C, B) fTCP sintered at 1200 °C, C) dTCP sintered at 1200 °C, D) PHO, E) dTCP/PHO, F) Phase composition of the obtained ceramic sinters, G,H) FTIR spectra of pure PHO, dTCP and dTCP/PHO composite.

hydroxyoctanoic acid 301.2→159.1 m/z, F = 63V, CE = 2V. MassHunter software (Agilent) was used for HPLC-MS system control, data acquisition, and data processing.

3. Results and discussion

3.1. Physicochemical studies of materials

Specific surface area (SSA) calculated for non-calcined powder was 71.76 ± 0.13 m² g⁻¹, whereas for calcined powder – 5.29 ± 0.02 m² g⁻¹. The average crystallite size of calcined β-TCP powder (computed with Scherrer's formula) was found to be 134.1 ± 1.4 nm. The calcined powder was used as the initial powder for foams as it needed less liquid content during ceramic slurry preparation leading to foams with fewer microcracks. Attempts to obtain macroporous scaffolds without pre-calcination of the powder were unsuccessful as they were more brittle than those obtained from calcined powder. Thermal treatment in air of the low-temperature amorphous-TCP phase (initially synthesized powder) at 900 °C for several hours did lead to the formation of 100% pure βTCP (Fig. 1A) which is in agreement with other studies (Kokubo, 2008).

After sintering the materials at 1200 °C XRD analysis revealed that part of the β-TCP was converted into α-TCP (Fig. 1B–C) which is associated with the starting transition temperature from β→α tricalcium phosphate phase above 1125 °C (Welch, 1961). Calcined powder showed a much lower β→α conversion (i.e. 3% for microporous samples, results not shown). In the case of macroporous specimens, the β→α conversion was greater if compared to the non-calcined powder (81% against 19%, respectively) (Fig. 1F). XRD analysis did not reveal appearance of any other phase. Higher β→α transition in the case of macroporous samples could be caused by the burning out the polyurethane sponge, during which the gas atmosphere is raised (Piszczyk et al., 2014).

Diffraction studies revealed that the ceramic material was characterized by high crystallinity, whereas pure PHO polymer possessed

diffractogram typical for the semi-crystalline polyhydroxyalkanoates (Moursi et al., 1997) (Fig. 1C–D). The ceramic discs coated with polymer combined features of both materials –crystalline TCP peaks with anamorphous halo originating from PHO(Fig. 1E). However, no characteristic crystalline reflections from PHO were observed. This may be due to a very thin polymer layer on microporous TCP disc.

Infrared spectroscopy studies conducted for dTCP sample revealed the presence of the bands characteristic for apatitic tricalcium phosphates phase. In the region of 1200-900 cm⁻¹ the spectrum of dTCP shows bands assigned to the stretching vibrations (ν) of PO₄³⁻ group. The band at ~960 cm⁻¹ and ~940 cm⁻¹ proved the presence of pure TCP (Nahar et al., 2017). The vibrations in the 600–660 cm⁻¹ range were results from bending vibration of PO₄³⁻ group. The presence of the bands at ~670 cm⁻¹ and ~605 cm⁻¹ might indicated bending vibration of PO₄³⁻ groups (Mirhadi et al., 2011). The spectrum of polyhydroxyoctanoate (PHO) revealed the typical structure of polyesters, as described previously (Shishatskaya et al., 2014). The intense absorption band at ~1730 cm⁻¹ corresponds to the stretching vibration of the ester carbonyl group (C=O). The bands between ~2950 cm⁻¹ and ~2850 cm⁻¹ are attributed to the stretching modes of CH₃ and CH₂ groups. The band at ~730 cm⁻¹ are assigned to the CH₂ groups, which are located in the side-chain of polyhydroxyoctanoate. The bands between ~1300 cm⁻¹ and ~1000 cm⁻¹ correspond to stretching mode of C-O-C groups. Deposition of PHO layer on the dTCP surface resulted in creation of the similar spectra as in case of pure PHO, thus confirms uniform coverage of the TCP ceramic disc by the polymer (Fig. 1G-H).

3.2. Surface characterization and 3D reconstruction

In order to confirm the coverage of ceramic sinters with a polymer layer microscopic observations (optical and SEM) were conducted. The presence of the polymer layer was already clearly visible under the optical microscope. However, the concentration of polymer solution used for coating did not affect ceramic surface significantly (Fig. 2). Microporous TCP discs immersed in PHO solutions were covered with
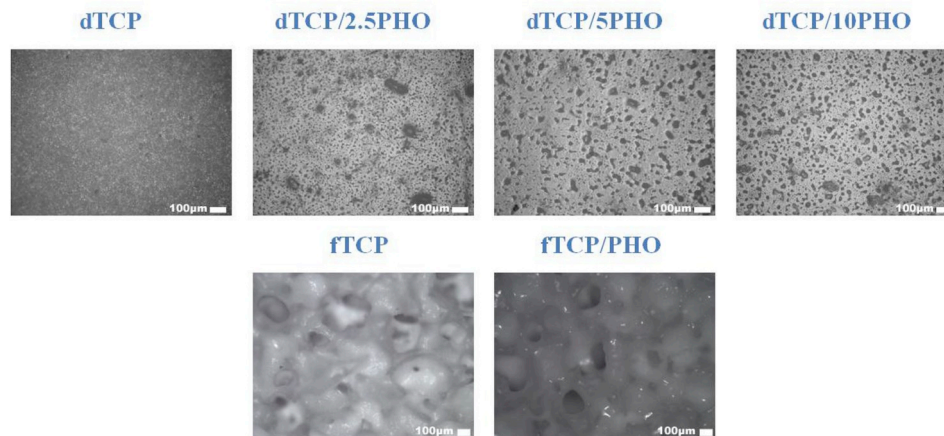
Fig. 2. Images from the optical microscope of dTCP, dTCP/PHO, fTCP and fTCP/PHO samples.

pores formed in the polymer layer due to evaporation of the solvent. It was also noticed that macroporous composite foams possessed a shiny glow due to the presence of the polymer (Fig. 2).

3.3. Determination of wettability and surface free energy (SFE) of the materials

The surface hydrophilicity of the samples was determined by water contact angle measurements. The surface properties, determined by free surface energy and measurements of materials wettability with potential applications in medicine, play an important role in tissue engineering and regenerative medicine. The surface hydrophilicity directly influences the biological performance of materials such as protein adsorption, attachment, migration and cell proliferation (Bretcanu et al., 2009). The presence of PHO coating on dTCP caused an increase of the contact angle, altering its superficies character from hydrophilic (35 ± 6°) to hydrophobic (over 90°) (Table 1). There were no significant differences between composite samples, which is an additional proof of the total dTCP sample coverage by the polymer. Additionally, the measured water contact angle of PHO (100 ± 6°) was similar to this reported in the literature (98 ± 2°) and also for other mcl-PHAs such as poly(3-hydroxyundecanoate) (PHUA) (100 ± 2°) (Mauclaire et al., 2010). It is worth mentioning that a polymer surface with a water contact angle of 70° is the most suitable surface for cell adhesion (Tamada and Ikada, 1993).

After application of polymer coating, the hydrophilic ceramic surface changed to a hydrophobic one. Generally, protein adsorption is greater on hydrophobic surfaces if compared to hydrophilic. Protein adsorption is an essential factor, taking into consideration interactions between biomaterial and cell or human body, as proteins are adsorbed faster than cells and often govern how the cells will attach to biomaterial's surface (Gentleman and Gentleman, 2014). The opposite is with proteins from the integrin family. Integrins are proteins that mediate cell adhesion to extracellular matrix (ECM) which are often taken into account as indicators of osteoblast behavior (cell attachment and proliferation) (Moursi et al., 1997). In the study on human foetal

osteoblastic cells (HFOC) conducted by Lim et al. integrins possessed significantly lower expression on hydrophobic surfaces. However, their findings did not correlate with osteoblast-specific gene expression, which is essential for appropriate differentiation and bone tissue formation. For example, a protein in bone – osteopontin, often used as a marker for osteoblastic differentiation, were higher in HFOC cultured on hydrophobic silane-treated quartz's surface compared to more hydrophilic ones (Lim et al., 2005). For the above-mentioned reasons we can assume that the change of surface character from hydrophilic to hydrophobic might have a quite positive effect.

The surface free energy (SFE) was determined according to equations listed in Section 2.8 and the results were collected in Table 1. The polar component of SFE was higher than the dispersive only for dTCP surfaces. However, the opposite results have been obtained by dos Santos et al. (Dos Santos et al., 2008), who showed that for TCP as well as for HAp the value of the polar component was lower than that of the dispersive. This discrepancy may be due to the fact that our materials contains numerous micropores on the dTCP surfaces that act as capillaries drawing water into the sample. In case of composite materials, the polymer coating on the ceramic surface resulted in a significant reduction of the polar component, while the dispersion component was slightly increased. This is due to changes in the surface wettability of the investigated materials. Total SFE of the uncoated microporous disc was two-fold higher [60.98 ± 3.60 (mN m^{-1})] than the total SFE for composites and PHO film [approx. 30 (mN m^{-1})]. Many reports suggest that high SFE promotes cell adhesion (Hallab et al., 2001; Baier et al., 1984), however research conducted for PHAs reveals it is not the case. Wang et al. reported that a copolymer of 3-hydroxybutyrate and 3-hydroxyhexanoate (PHBHHx) was a good cytocompatible material that allowed adhesion, proliferation and differentiation of osteogenic cells, outperforming much stiffer polymers – polyhydroxybutyrate and polylactide (Wang et al., 2004). Another example supporting this statement were *in vivo* tests conducted for 3D implants from P3HB and composites of P3HB/HA that showed noticeable osteoplastic properties with normal reparative osteogenesis (Shishatskaya et al., 2014).

Table 1
Wetting properties, components of SFE and SFE for investigated dTCP and PHO surfaces.

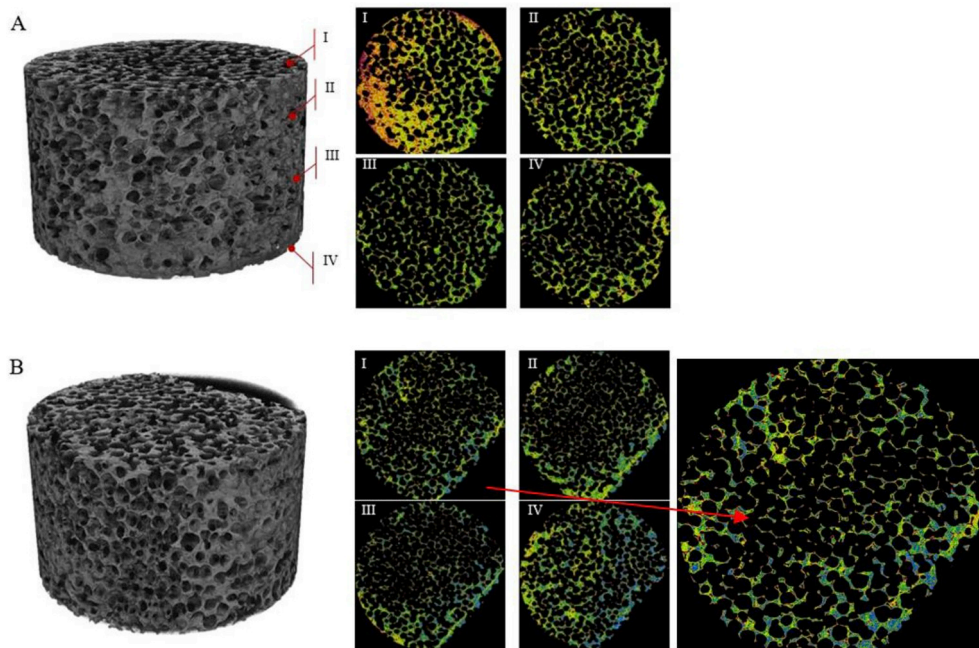| Samples	Water contact angle (°)	Diiodomethane contact angle (°)	Polar surface free energy (mN m^{-1})	Dispersive surface free energy (mN m^{-1})	Total surface free energy (mN m^{-1})
dTCP	35 ± 6	38 ± 4	34.16 ± 4.55	26.82 ± 1.69	60.98 ± 3.60
dTCP/2.5PHO	93 ± 1	56 ± 3	1.93 ± 0.43	27.93 ± 2.28	29.76 ± 1.89
dTCP/5PHO	94 ± 2	56 ± 5	1.30 ± 0.57	30.79 ± 3.29	32.09 ± 2.88
dTCP/10PHO	91 ± 2	60 ± 5	2.26 ± 0.92	28.39 ± 1.50	30.65 ± 1.32
PHO	100 ± 6	52 ± 3	0.92 ± 0.04	33.36 ± 0.12	34.40 ± 0.10

Fig. 3. μCT scans of the obtained scaffolds: A) fTCPB) fTCP/PHO (with iodobenzene). I, II, III and IV stand for their cross-sections.

3.4. Infiltration efficiency and architecture of the scaffolds

Studies performed by computer micro-tomography (μCT) clearly showed the macroporous architecture of the scaffolds (Fig. 3). The pores were interconnected, which is a crucial feature of a given scaffold for its use in BTE. PHO presence in fTCP/PHO scaffolds was confirmed by a blue colour (from iodide). Despite the infiltration with the polymer, the porous architecture of the foams was preserved.

3.5. Microstructure

In order to visualize the microstructure of the flat dTCP and their composites SEM photomicrographs were taken (Fig. 4A–D). In addition, cross-sections of studied flat materials were investigated to determine the thickness of the polymer layer (Fig. 4E–H). The polymer was clearly visible on the surface of all composite materials. At lower PHO concentrations embedded TCP grains were visible (Fig. 4B-C), whereas for dTCP/10PHO the TCP grains were no longer noticeable (layer thickness > 200 μm) (Figs. 4D and 5H). Such a thick polymer layer in case of scaffolds is not a beneficial phenomenon, as it would probably lead to clogging of the pores that are < 400 μm. On the other hand, it can be seen that in case of dTCP/2.5PHO composite it is not possible to clearly indicate the PHO layer (Fig. 4E). However, the most promising result was obtained for dTCP/5PHO, where PHO layer was somewhat around 30 μm (Fig. 4G). This order of film thickness should not interfere with osteoblast interaction with the ceramic base of the scaffold as it was proven previously that cells sense the main support still if polymer modification (in our case PHO) is not greater than 100 μm (Sicchieri et al., 2012; Hannink and Arts, 2011). Taking the above under consideration 5 wt% polymer solution was used for the immersion of foams. EDS analysis in microareas of the composite cross-section confirmed its chemical composition (Fig. 4I-J).

All of the studied ceramic foams were very well sintered. This was evidenced by the good adhesion of pores and the absence of microcracks – even on the cross-sections of foams. The above-mentioned features make the material less brittle and durable, which is extremely important in design of highly porous ceramics. Microstructure observations of ceramic foams (Fig. 4K-N) revealed intrinsic porosity in two ranges: large pores (200 – 700 μm) and small pores (50 – 200 μm),

which is similar to these obtained by us previously (Ślósarczyk et al., 2010). In case of composite foams (fTCP/PHO) the PHO layer was clearly visible. The polymer detachment from the ceramic surface was also observed (Fig. 4M-N). Some pores were not covered with a polymer layer. Most likely they were closed pores and only opened during sample cross-sectioning (Fig. 4N). The observed pore size of ~100 μm wide and the presence of the interconnected porosity in the fTCP/PHO scaffolds indicates the suitability of the materials for cell attachment, proliferation, migration, as well as vascularization based on other reports (Freyman et al., 2001).

3.6. Porosity

Apparent density, open and total porosity are shown in Table 2. Results revealed that ceramic scaffolds (fTCP) possessed about 56% of open porosity, which was close to its total porosity (60%). However, in case of infiltrated material (fTCP/PHO) we observed a slight decrease of open porosity to 52%. The reduction of open porosity probably resulted from clogging of some smaller pores by the polymer. Nevertheless, clogged pores may be opened after some time due to the degradation of PHO. The optimum pore size, which promotes the bone ingrowth and supports its regeneration should exceed at least $50\,\mu m^3$. On the basis of optical microscopy observations, it has been assumed that our macroporous materials met that requirement for the fact that the fTCP mean pore diameter was $416 \pm 252\,\mu m$, while fTCP/PHO – $254 \pm 45\,\mu m$. The reduced pore diameter was caused by the lining polymer. The porosity was also calculated on the basis of scans obtained from μCT method and was 79 and 78 vol % for fTCP and for fTCP/PHO, respectively. The pore size distribution and their visualizations are shown in the Fig. 5. Based on histograms of pores diameter we can assume that that in the obtained foams, apart from macropores (> 100 μm), also numerous micropores (< 100 μm) were present. Many researchers postulated that the presence of macro- and microporosity can lead to multiscale osteointegration (Levengood et al., 2010).

3.7. Compressive strength and mechanical properties

The compressive strength of studied macroporous materials was $6.0 \pm 1.8\,MPa$ and $6.7 \pm 2.5\,MPa$ for fTCP and fTCP/PHO,
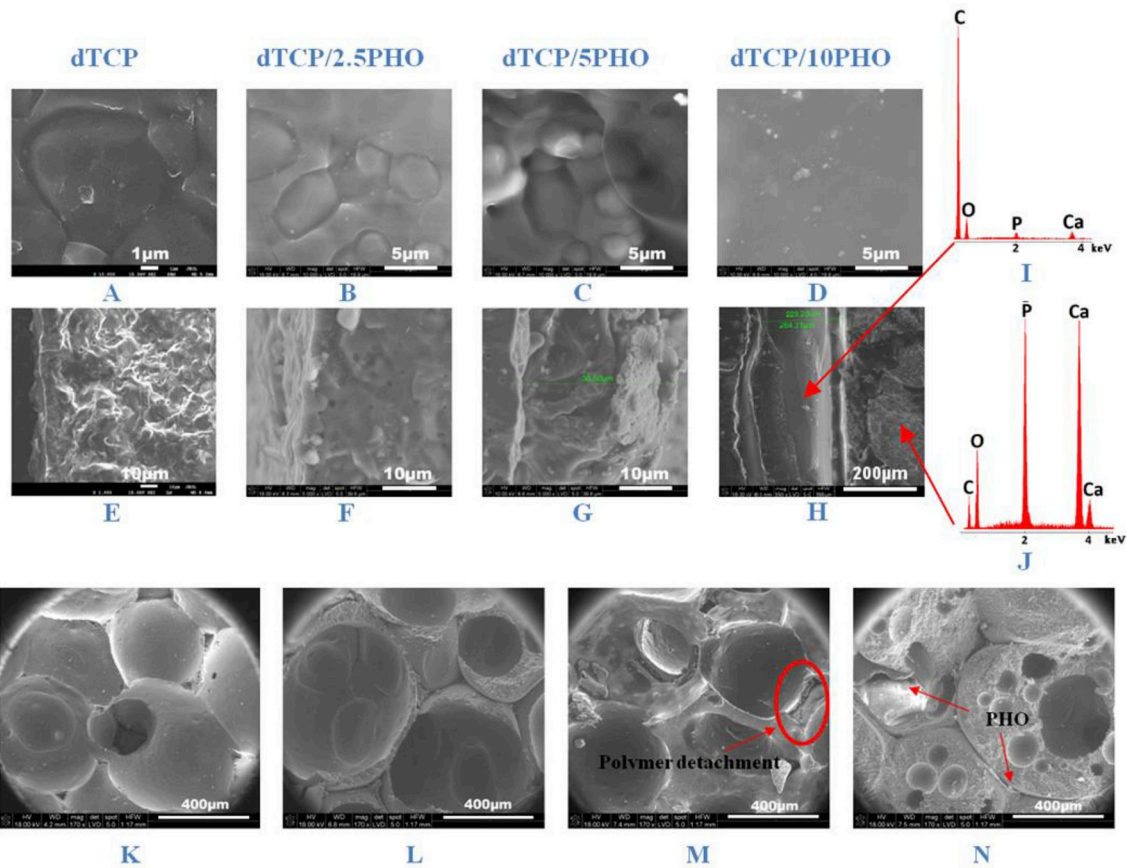
Fig. 4. SEM images of surface (A-D) and cross-section (E-H), EDS analysis in microareas of dTCP/10PHO cross-section (I - J). SEM images of foams: K) fTCP surface, L) cross-sectionof fTCP and M) fTCP/PHO surface, N)cross-section of fTCP/PHO.
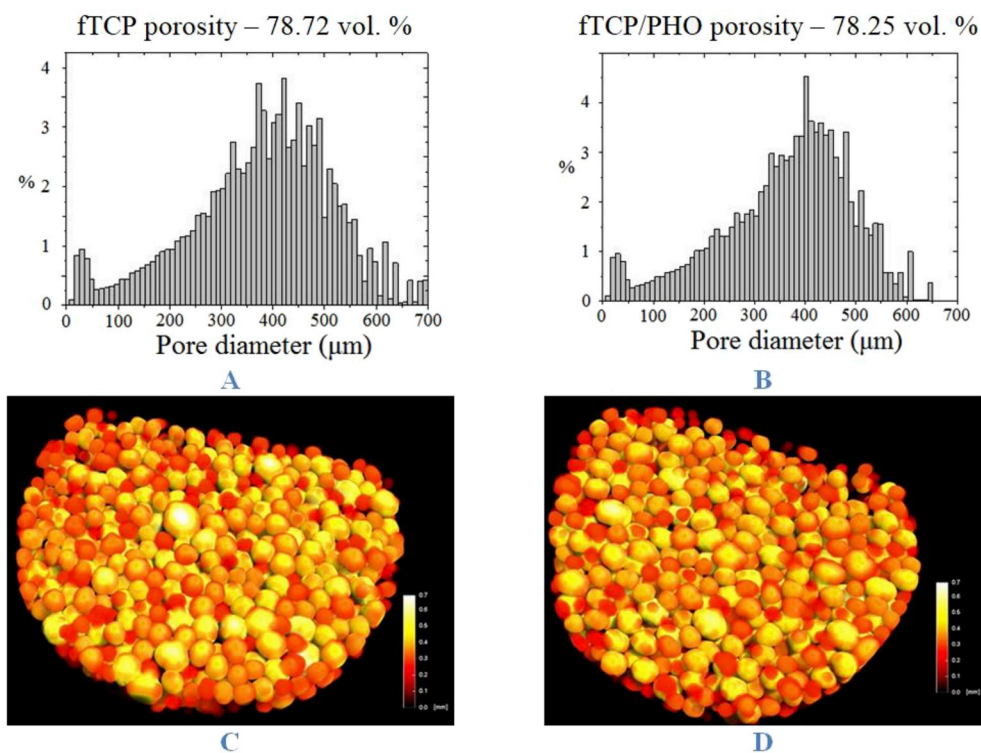

Fig. 5. Pore size distribution A) fTCP, B) fTCP/PHO and pore visualization (from dark red 0 mm to pale yellow 0.7 mm) C) fTCP, D) fTCP/PHO.

Table 2
Apparent density, open and total porosity of the obtained scaffolds based on Archimedes method.

Samples	Apparent density [g cm^{-3}]	Open porosity [vol. %]	Total porosity [vol. %]
fTCP - AM	1.17 ± 0.14	55.71 ± 4.81	61.22 ± 4.56
fTCP/PHO - AM	1.31 ± 0.08	52.26 ± 1.64	59.18 ± 2.60

respectively. These values meet the requirements for applications as a substitute forcancellous bone tissue (1.5 – 38.0 MPa) (Martin et al., 2015). Stress-strain characteristics of the obtained materials differed from the typical characteristics of the brittle ceramic materials. In most of the PHO-infiltrated foams a plateau region following the maximum load was observed, similar as in the case of other polymer-infiltrated ceramic foams described in the literature (Kang et al., 2011). The presence of the polymer had a noticeable effect on the cohesion and mechanical properties as well as on the durability of the constructs. The fTCP samples after compressive test formed a lot of debris disintegrating into small pieces (Fig. 6C), whereas the fTCP/PHO composites remained good integrity (Fig. 6D). The lack of debris is very important from the BTE point of view because they can lead to granulomas and

further to general inflammation (Van der Meulen and Koerten, 1994). Elasticity and durability of the obtained composites can be explained by the polymeric microfilaments that combine ceramic cracks like bridges and prevent constructs destruction (Fig. 6E-F). Similar effects of the beneficial influence of polymer infiltration of ceramic foams were described in several studies (Philippart et al., 2015).

3.8. Chemical stability and in vitro bioactivity studies in simulated body fluid

The chemical stability and bioactivity of composite discs were examined by their soaking in Simulated Body Fluid (SBF). Chemical stability of the studied materials based on measurements of SBF pH during the study did not reveal any alterations of its value, which persisted in the range 7.3 - 7.7, despite a coating with the polymer that degrades to (R)-3-hydroxyacids and their oligomers. After 21-day of incubation in SBF the changes of the samples surface microstructure and composition were noticed. This treatment induced formation of the apatite-like layer (Fig. 7B). It should be noted that before incubation in SBF the apatite layer was not recognizable on the surface of the studied samples (Fig. 7A). Negligible precipitation level of apatite phase was observed for unmodified dTCP surface which is in agreement with other studies
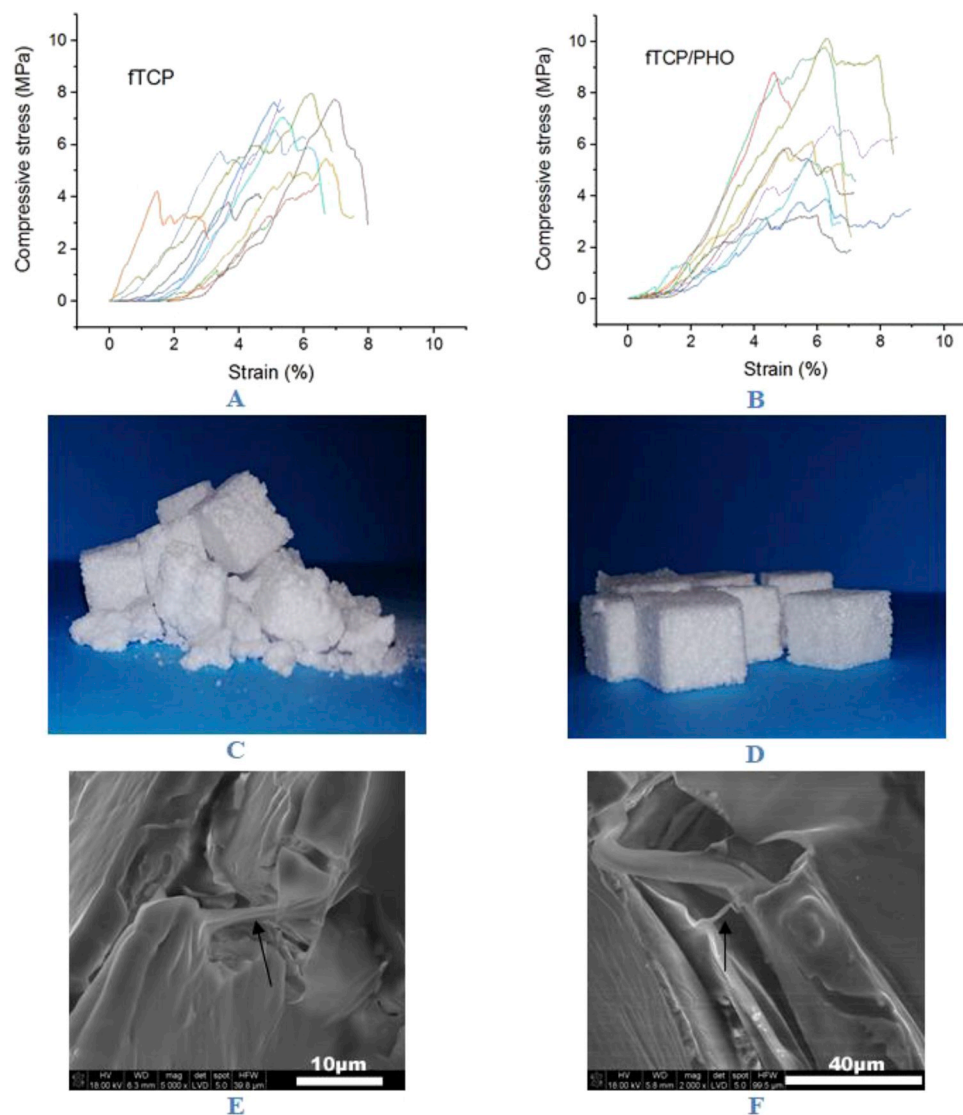

Fig. 6. Compressive stress in function of strain of the obtained scaffolds: A) fTCP, B) fTCP/PHO; samples after compression test: C) fTCP, D) fTCP/PHO; E) and F) SEM microphotographs of PHO microfilaments connecting ceramics' cracks like bridges (arrows) in fTCP/PHO material.
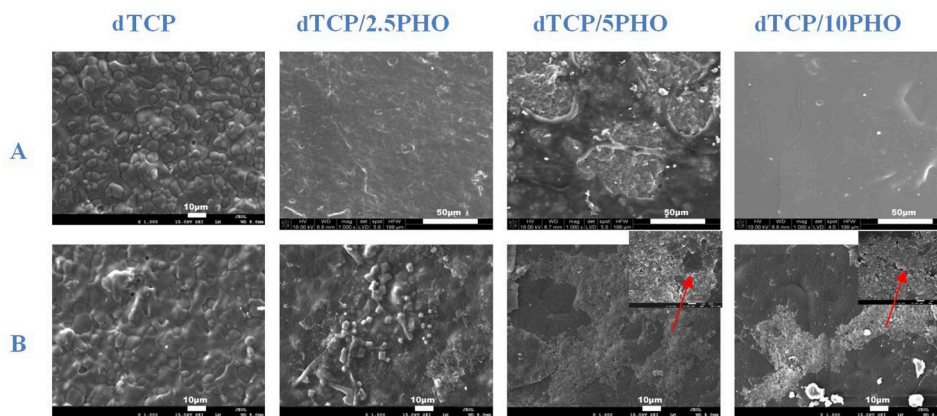
Fig. 7. SEM images of discs' surface: A) before incubation in SBF - magnification 1000x) B) after 21-day incubation in SBF - magnification 1000x (arrows indicate additional magnification 10000x).

where the β-TCP phase behaves as an 'inert'' material in SBF since it possesses the lower potential of bone-like apatite formation when compared to α-TCP (Bohner and Lemaitre, 2009). On the inorganic/organic discs surfaces, especially dTCP/5PHO and dTCP/10PHO an extensive apatite layer had formed. Interestingly, it was also possible to see a typical 'cauliflower' morphology of bone-like apatite layer in SEM images with higher magnification. These results confirmed that elastomeric polyhydroxyoctanoate coating on dTCP fosters the formation of an apatite-like layer on the material surface. It is in agreement with previous work where another polyhydroxyalkanoate - brittle polyhydroxybutyrate (PHB) was used (Szubert et al., 2014). Chemical stability and bioactivity depends strongly on choice of buffer. During interpretation, however, note that comparisons between studies in different media are problematic and absolute statements indicating that this type of material is bioactive or not should be treated with caution (Shah et al., 2014; Rohanová et al., 2018). It should be taken into account that the results obtained in one medium - in our case in SBF are not unambiguous and for the purpose of their final confirmation further research is needed.

3.9. Degradation studies

The degradation rate is another very important factor describing the biomaterials used for the production of scaffolds for bone tissue engineering, as it needs to correlate with bone own rate of regeneration. Moreover, the products of material degradation have a significant effect on the processes occurring during healing and new bone formation (Alsberg et al., 2003). For above-mentioned reasons studied materials were subjected to hydrolytic degradation studies in order to observe, analyze and evaluate changes in their microstructure, as well as to determine their degradation products. Microstructure changes after 92-day incubation in distilled water were observed in all of the investigated materials (Fig. 8). The surface of microporous TCP disc without polymer coating was not so homogenous as before incubation in water and possessed many gaps, probably caused by dissolution of the material. TCP/2.5PHO sample no longer had a continuous polymer layer but many voids could be noticed. Moreover, some microcracks in the polymer layer were observed (TCP/2.5PHO and TCP/5PHO samples). Additionally, on the surface of TCP/5PHO sample grains, which were not visible before incubation in water could be already noticed (Fig. 8A). PHO layer on TCP/10PHO surface after the time of experiment was still relatively continuous but a significant difference in the thickness of the layer could be noticed on its cross-section (from > 200 μm before and about 70 μm post degradation) (Fig. 8B). Obtained results confirmed the degradation of investigated materials making them excellent candidates for temporal bone tissue scaffolds.

3.10. Release study of polyhydroxyoctanoate components

Samples supernatants derived from SBF and degradation studies were analysed with HPLC-MS, which enabled us to identify the degradation components of the PHO films. The MS/MS analyses confirmed that the polymer degraded into not only pure (R)-3-hydroxyalted fatty acids but also to their dimers and trimers that contained both (R)-3-hydroxyhexanoic and (R)-3-hydroxyoctanoic acids (see: supplementary materials). Predominantly the fatty acid dimers were formed, with the main of (R)-3-hydroxyoctanoate-(R)-3-hydroxyoctanoic acid. Analogically, the most abundant signal for single fatty acids corresponded to the (R)-3-hydroxyoctanoic. The concentrations of these components were unquantifiable, as were below the limit of quantification of our apparatus (level below ng L^{-1}). The slow release of PHO components to SBF did not alter its pH and thus is a good indication of nourishing character of the used polymer.

4. Overall discussion

So far, some composites in the form of highly biocompatible and commonly used calcium phosphates coated with short chain length polyhydroxyalkanoates have been tested. Application of PHA coating had a positive influence on compressive strength, bioactivity, cell proliferation rate (Poirier et al., 1995; Ray et al., 2019). However, to date, an elastomeric mcl-PHA representative, namely polyhydroxyoctanoate, which presents absolutely different characteristics than PHB, was not used as a coating in BTE applications. What is more, we established that the obtained materials are degradable and their degradation products may nourish the developing tissue, thus making them good candidates as temporal scaffolds in BTE. Obtained in this study composites in future may also be used as small molecule carriers – novel materials for delivering therapeutic drugs (Mouriño and Boccaccini, 2009), antibiotics to prevent infections and growth factors to enhance new bone formation (Yoshida et al., 2015).

5. Conclusions

The composite materials (microporous discs and macroporous foams) consisting of tricalcium phosphate and polyhydroxyoctanoate were obtained successfully. We have determined the concentration of a polymer solution (5% w/v) in which the macroporous ceramic could be successfully immersed and mostly infiltrated. We confirmed the positive effect of the PHO on the physicochemical properties of TCP scaffolds. The polymer layer enhanced the wettability towards more cell-friendly material. Moreover, durability of the composites was enhanced (stress-strain characteristics) by infiltration with the PHO polymer, which can also act as nourishing compound as well as drug carrier.
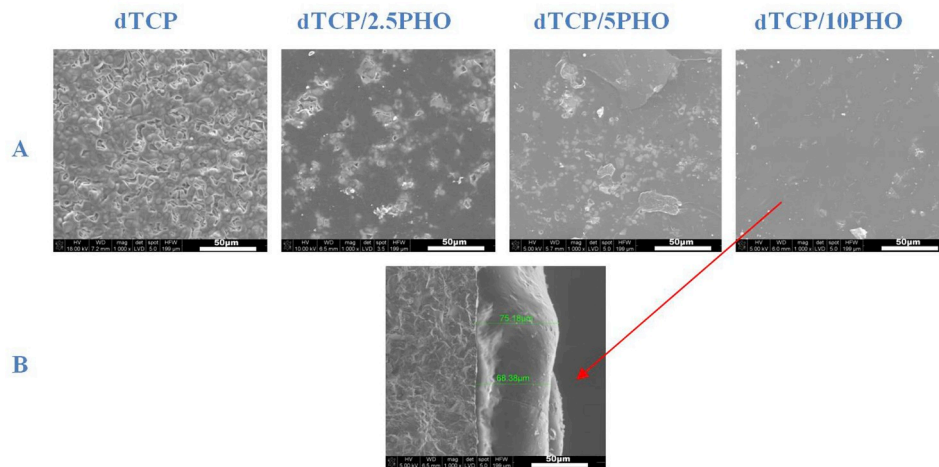
Fig. 8. SEM images of discs after 92-days of hydrolytic degradation (magnification 1000x): A) surfaces, B) cross-section through TCP/10PHO sample (magnification 1000x).

Despite extensive research on the properties of the materials obtained in this study, further research is needed – in particular *in vitro* and *in vivo* behaviour of these novel composites should be investigated.

Acknowledgements

Appendix A. Supplementary data

Supplementary data to this article can be found online at https://doi.org/10.1016/j.jmbbm.2019.06.028.

References

Alsberg, E., Kong, H.J., Hirano, Y., Smith, M.K., Albeiruti, A., Mooney, D.J., 2003. Regulating bone formation via controlled scaffold degradation. J. Dent. Res. 82 (11), 903–908.
Baier, R.E., Meyer, A.E., Natiella, J.R., Natiella, R.R., Carter, J.M., 1984. Surface properties determine bioadhesive outcomes: methods and results. J. Biomed. Mater. Res. 18 (4), 337–355.
Blokhuis, T.J., Termaat, M.F., den Boer, F.C., Patka, P., Bakker, F.C., Henk, J.T.M., 2000. Properties of calcium phosphate ceramics in relation to their in vivo behavior. J. Trauma Acute Care Surg. 48 (1), 179.
Bohner, M., Lemaitre, J., 2009. Can bioactivity be tested in vitro with SBF solution? Biomaterials 30 (12), 2175–2179.
Bretcanu, O., Chen, Q., Misra, S.K., Boccaccini, A.R., Roy, I., Verne, E., Brovarone, C.V., 2007. Biodegradable polymer coated 45S5 Bioglassderived glass-ceramic scaffolds for bone tissue engineering. Glass Technol. Eur. J. Glass Sci. Technol. A 48 (5), 227–234.
Bretcanu, O., Misra, S., Roy, I., Renghini, C., Fiori, F., Boccaccini, A.R., Salih, V., 2009. In vitro biocompatibility of 45S5 Bioglass®-derived glass–ceramic scaffolds coated with poly (3-hydroxybutyrate). J. Tissue Eng. Regenerat. Med. 3 (2), 139–148.
Doebelin, N., Kleeberg, R., 2015. Profex: a graphical user interface for the Rietveld refinement program BGMN. J. Appl. Crystallogr. 48 (5), 1573–1580.
Dos Santos, E.A., Farina, M., Soares, G.A., Anselme, K., 2008. Surface energy of hydroxyapatite and β-tricalcium phosphate ceramics driving serum protein adsorption and osteoblast adhesion. J. Mater. Sci. Mater. Med. 19 (6), 2307–2316.
Freyman, T.M., Yannas, I.V., Gibson, L.J., 2001. Cellular materials as porous scaffolds for tissue engineering. Prog. Mater. Sci. 46 (3–4), 273–282.

Fu, Q., Jia, W., Lau, G.Y., Tomsia, A.P., 2018. Strength, toughness, and reliability of a porous glass/biopolymer composite scaffold. J. Biomed. Mater. Res. B Appl. Biomater. 106 (3), 1209–1217.
Gadgil, B.S.T., Killi, N., Rathna, G.V., 2017. Polyhydroxyalkanoates as biomaterials. MedChemComm 8 (9), 1774–1787.
Garcea, S.C., Wang, Y., Withers, P.J., 2018. X-ray computed tomography of polymer composites. Compos. Sci. Technol. 156, 305–319.
Gentleman, M.M., Gentleman, E., 2014. The role of surface free energy in osteoblast–biomaterial interactions. Int. Mater. Rev. 59 (8), 417–429.
Goreva, A.V., Shishatskaya, E.I., Volova, T.G., Sinskey, A.J., 2012. Characterization of polymeric microparticles based on resorbable polyesters of oxyalkanoic acids as a platform for deposition and delivery of drugs. Polym. Sci. 54 (2), 94–105.
Gould, P.L., Holland, S.J., Tighe, B.J., 1987. Polymers for biodegradable medical devices. IV. Hydroxybutyrate-valerate copolymers as non-disintegrating matrices for controlled-release oral dosage forms. Int. J. Pharm. 38 (1–3), 231–237.
Hallab, N.J., Bundy, K.J., O'Connor, K., Moses, R.L., Jacobs, J.J., 2001. Evaluation of metallic and polymeric biomaterial surface energy and surface roughness characteristics for directed cell adhesion. Tissue Eng. 7 (1), 55–71.
Hannink, G., Arts, J.C., 2011. Bioresorbability, porosity and mechanical strength of bone substitutes: what is optimal for bone regeneration? Injury 42, S22–S25.
Kamitakahara, M., Ohtsuki, C., Miyazaki, T., 2008. Behavior of ceramic biomaterials derived from tricalcium phosphate in physiological condition. J. Biomater. Appl. 23 (3), 197–212.
Kang, Y., Scully, A., Young, D.A., Kim, S., Tsao, H., Sen, M., Yang, Y., 2011. Enhanced mechanical performance and biological evaluation of a PLGA coated β-TCP composite scaffold for load-bearing applications. Eur. Polym. J. 47 (8), 1569–1577.
Kokubo, T. (Ed.), 2008. Bioceramics and Their Clinical Applications. Elsevier.
Levengood, S.K.L., Polak, S.J., Wheeler, M.B., Maki, A.J., Clark, S.G., Jamison, R.D., Johnson, A.J.W., 2010. Multiscale osteointegration as a new paradigm for the design of calcium phosphate scaffolds for bone regeneration. Biomaterials 31 (13), 3552–3563.
Lim, J.Y., Taylor, A.F., Li, Z., Vogler, E.A., Donahue, H.J., 2005. Integrin expression and osteopontin regulation in human fetal osteoblastic cells mediated by substratum surface characteristics. Tissue Eng. 11 (1–2), 19–29.
Martin, R.B., Burr, D.B., Sharkey, N.A., et al., 2015. Skeletal Tissue Mechanics. Springer, New York (NY).
Mauclaire, L., Brombacher, E.B.J.D., Bünger, J.D., Zinn, M., 2010. Factors controlling bacterial attachment and biofilm formation on medium-chain-length polyhydroxyalkanoates (mcl-PHAs). Colloids Surfaces B Biointerfaces 76 (1), 104–111.
Mirhadi, B., Mehdikhani, B., Askari, N., 2011. Synthesis of nano-sized β-tricalcium phosphate via wet precipitation. Process. Appl. Ceram. 5 (4), 193–198.
Mouriño, V., Boccaccini, A.R., 2009. Bone tissue engineering therapeutics: controlled drug delivery in three-dimensional scaffolds. J. R. Soc. Interface 7 (43), 209–227.
Moursi, A.M., Globus, R.K., Damsky, C.H., 1997. Interactions between integrin receptors and fibronectin are required for calvarial osteoblast differentiation in vitro. J. Cell Sci. 110 (18), 2187–2196.
Murphy, C.M., Haugh, M.G., O'Brien, F.J., 2010. The effect of mean pore size on cell attachment, proliferation and migration in collagen–glycosaminoglycan scaffolds for bone tissue engineering. Biomaterials 31 (3), 461–466.
Nahar, U.K., Shovon, B., Chandra, R.D., Shukanta, B., Chandra, S.P., 2017. Characterization of beta-tricalcium phosphate (β-TCP) produced at different process conditions. J. Bioeng. Biomed. Sci. 7 (221), 2.
Philippart, A., Boccaccini, A.R., Fleck, C., Schubert, D.W., Roether, J.A., 2015. Toughening and functionalization of bioactive ceramic and glass bone scaffolds by biopolymer coatings and infiltration: a review of the last 5 years. Expert Rev. Med. Devices 12 (1), 93–111.
Piszczyk, Ł., Strankowski, M., Danowska, M., Hejna, A., Haponiuk, J.T., 2014. Rigid polyurethane foams from a polyglycerol-based polyol. Eur. Polym. J. 57, 143–150.

Poirier, Y., Nawrath, C., Somerville, C., 1995. Production of polyhydroxyalkanoates, a family of biodegradable plastics and elastomers, in bacteria and plants. Biotechnology 13 (2), 142.

Ray, S., Patel, S.K., Singh, M., Singh, G.P., Kalia, V.C., 2019. Exploiting poly-hydroxyalkanoates for tissue engineering. In: Biotechnological Applications of Polyhydroxyalkanoates. Springer, Singapore, pp. 271–282.

Raynaud, S., Champion, E., Bernache-Assollant, D., Thomas, P., 2002. Calcium phosphate apatites with variable Ca/P atomic ratio I. Synthesis, characterisation and thermal stability of powders. Biomaterials 23 (4), 1065–1072.

Renard, E., Walls, M., Guérin, P., Langlois, V., 2004. Hydrolytic degradation of blends of polyhydroxyalkanoates and functionalized polyhydroxyalkanoates. Polym. Degrad. Stabil. 85 (2), 779–787.

Rohanová, D., Horkavcová, D., Paidere, L., Boccaccini, A.R., Bozděchová, P., Bezdička, P., 2018. Interaction of HEPES buffer with glass-ceramic scaffold: can HEPES replace TRIS in SBF? J. Biomed. Mater. Res. B Appl. Biomater. 106 (1), 143–152.

Rossi, S., Azghani, A.O., Omri, A., 2004. Antimicrobial efficacy of a new antibiotic-loaded poly (hydroxybutyric-co-hydroxyvaleric acid) controlled release system. J. Antimicrob. Chemother. 54 (6), 1013–1018.

Shah, F.A., Brauer, D.S., Wilson, R.M., Hill, R.G., Hing, K.A., 2014. Influence of cell culture medium composition on in vitro dissolution behavior of a fluoride-containing bioactive glass. J. Biomed. Mater. Res. A 102 (3), 647–654.

Shishatskaya, E.I., Kamendov, I.V., Starosvetsky, S.I., Vinnik, Y.S., Markelova, N.N., Shageev, A.A., et al., 2014. An in vivo study of osteoplastic properties of resorbable poly-3-hydroxybutyrate in models of segmental osteotomy and chronic osteomyelitis. Artif. Cells Nanomed. Biotechnol. 42 (5), 344–355.

Sicchieri, L.G., Crippa, G.E., de Oliveira, P.T., Beloti, M.M., Rosa, A.L., 2012. Pore size regulates cell and tissue interactions with PLGA–CaP scaffolds used for bone engineering. J. Tissue Eng. Regenerat. Med. 6 (2), 155–162.

Ślósarczyk, A., Paszkiewicz, Z., 2005. Method of Obtaining Highly Reactive Calcium Phosphate Powder. Polish Patent PL190486B1.

Ślósarczyk, A., Potoczek, M., Paszkiewicz, Z., Zima, A., Lewandowska-Szumieł, M., Chróścicka, A., 2010. Fabrication, characteristics and biological evaluation of highly porous hydroxyapatite bioceramics. Materiały Ceramiczne/Ceram. Mater. 62 (2), 224–229.

Sofińska, K., Barbasz, J., Witko, T., Dryzek, J., Haraźna, K., Witko, M., et al., 2019. Structural, topographical, and mechanical characteristics of purified poly-hydroxyoctanoate polymer. J. Appl. Polym. Sci. 136 (4), 47192.

Szubert, M., Adamska, K., Szybowicz, M., Jesionowski, T., Buchwald, T., Voelkel, A., 2014. The increase of apatite layer formation by the poly (3-hydroxybutyrate) surface modification of hydroxyapatite and β-tricalcium phosphate. Mater. Sci. Eng. C 34, 236–244.

Tamada, Y., Ikada, Y., 1993. Effect of preadsorbed proteins on cell adhesion to polymer surfaces. J. Colloid Interface Sci. 155 (2), 334–339.

Van der Meulen, J., Koerten, H.K., 1994. Inflammatory response and degradation of three types of calcium phosphate ceramic in a non-osseous environment. J. Biomed. Mater. Res. 28 (12), 1455–1463.

Wang, Y.W., Wu, Q., Chen, G.Q., 2004. Attachment, proliferation and differentiation of osteoblasts on random biopolyester poly (3-hydroxybutyrate-co-3-hydro-xyhexanoate) scaffolds. Biomaterials 25 (4), 669–675.

Welch, J.H., 1961. High-temperature studies of the system calcium oxide-phosphorus pentoxide. J. Chem. Soc. 4442–4444.

Winkler, T., Sass, F.A., Duda, G.N., Schmidt-Bleek, K., 2018. A review of biomaterials in bone defect healing, remaining shortcomings and future opportunities for bone tissue engineering: the unsolved challenge. Bone Joint Res. 7 (3), 232–243.

Yoshida, T., Miyaji, H., Otani, K., Inoue, K., Nakane, K., Nishimura, H.,, et al., 2015. Bone augmentation using a highly porous PLGA/β-TCP scaffold containing fibroblast growth factor-2. J. Periodontal. Res. 50 (2), 265–273.